The Role of Standing Waves in Driving Persistent Anomalies of Upward Wave Activity Flux

OLIVER WATT-MEYER AND PAUL J. KUSHNER

Department of Physics, University of Toronto, Toronto, Ontario, Canada

(Manuscript received 30 April 2015, in final form 22 September 2015)

ABSTRACT

Northern Hemisphere stratospheric polar vortex strength variability is known to be largely driven by persistent anomalies in upward wave activity flux. It has also been shown that attenuation and amplification of the stationary wave is the primary way in which wave activity flux varies. This study determines the structure of the wave anomalies that interfere with the climatological wave and drive this variability. Using a recently developed spectral decomposition it is shown that fixed-node standing waves are the primary drivers of the ''linear interference'' phenomenon. This is particularly true for the low-frequency component of the upward wave activity flux. The linear part of the flux is shown to be more persistent than the total flux and has significant tropospheric standing wave precursors that lead changes in the strength of the stratospheric polar vortex. Evidence is presented that current-generation high-top climate models are able to credibly simulate this variability in wave activity fluxes and the connection to polar vortex strength. Finally, the precursors to displacement and split sudden stratospheric warmings are examined. Displacement events are found to be preceded by about 25 days of anomalously high upward wave activity flux forced by standing waves amplifying the climatology. Split events have more short-lived wave activity flux precursors, which are dominated by the nonlinear part of the flux.

1. Introduction

The predictability of extreme stratospheric polar vortex events in the Northern Hemisphere winter is a topic of current research (Tripathi et al. 2015) due to their significant impact on tropospheric weather on the time scales of weeks to months (Baldwin and Dunkerton 2001; Thompson et al. 2002; Sigmond et al. 2013). Weakening and strengthening of the polar vortex are known to be preceded by, respectively, persistent positive and negative anomalies of upward wave activity flux in the lower stratosphere (Newman et al. 2001; Polvani and Waugh 2004). A number of studies have emphasized the sensitivity of mean-flow variability in the stratosphere to the time scale of wave activity pulses (Harnik 2009; Sjoberg and Birner 2012, 2014). In particular, Harnik (2009) showed that shorter pulses of upward wave activity resulted in wave reflection in the upper stratosphere and no long-lasting deceleration of the polar vortex, whereas longer pulses forced a sudden stratospheric warming (SSW)-like response, with a downward propagation of zonal mean wind anomalies through the stratosphere. Sjoberg and Birner (2012, 2014) explored the importance of the duration of wave activity pulses in driving weakening in the strength of the polar vortex. They showed both in reanalysis and through simple modeling experiments that the stratosphere is especially responsive to positive anomalies of wave activity flux lasting 10 to 20 days. This suggests that understanding the mechanisms that tend to drive pulses of this longer time scale is essential for improving the prediction of SSWs.

The ''linear interference'' framework is a useful way to understand the variability of upward wave activity flux and the driving of polar vortex events (Nishii et al. 2009; Garfinkel et al. 2010; Smith and Kushner 2012). This method separates flux anomalies—we will focus on meridional eddy heat flux as a proxy for upward wave activity—into a contribution that is due to the interference of wave anomalies with the background climatological wave (we call this the LIN term) and another term that is solely due to interactions of the wave anomaly with itself (we call this the NONLIN

Corresponding author address: Oliver Watt-Meyer, Department of Physics, University of Toronto, 60 St. George St., Toronto, ON M5S 1A7, Canada.
E-mail: oliverwm@atmosp.physics.utoronto.ca

DOI: 10.1175/JCLI-D-15-0317.1

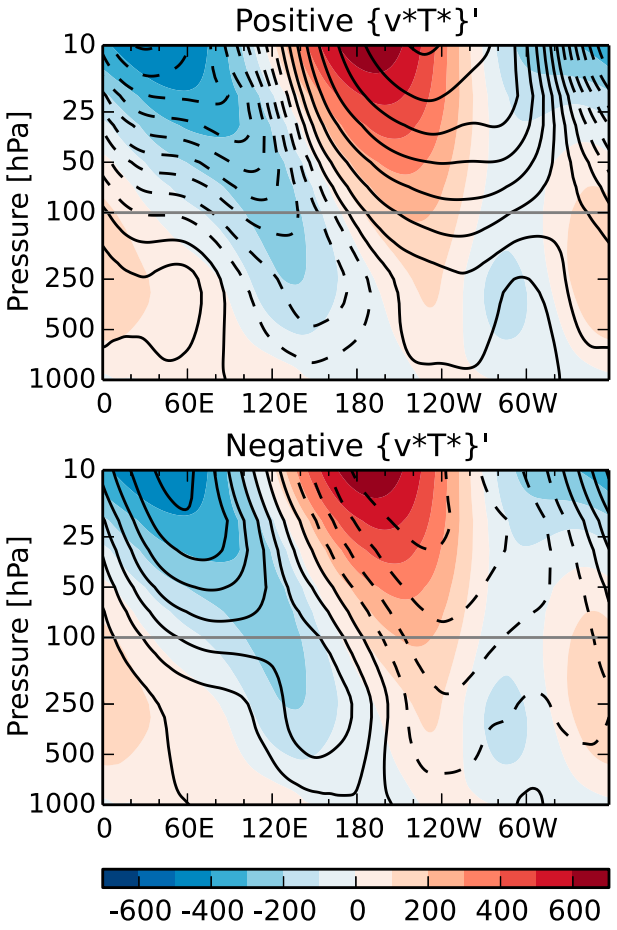

FIG. 1. Shading: NDJFM Z_c^* at 60°N, in units of m. Contours: $Z^{*\prime}$ at 60°N, composited over days of anomalously (top) high and (bottom) low heat flux at 60°N and 100 hPa. The particular days selected for compositing are the period of most extreme 10-day averaged heat flux anomaly over each NDJFM season. The contour line intervals for $Z^{*\prime}$ are 40 m with dashed lines negative and solid lines zero or positive.

term). The motivation for this decomposition comes from the fact that, as shown in Fig. 1, periods of anomalously large and small upward wave activity flux correspond to wave anomalies being in and out of phase with the climatological wave.[1] This suggests that the relative phasing of wave anomalies and the background climatology, which is quantified by the LIN term, is an important determiner of the heat flux anomaly. Smith and Kushner (2012) examined the characteristics of the LIN and NONLIN terms, and their relative roles in initiating stratosphere–troposphere interactions. Their primary conclusions were that the LIN term explains the largest portion of the interannual variability of anomalous heat flux in both hemispheres' winters, and that the LIN term is driven by low-frequency, planetary-scale (wavenumbers 1 and 2, primarily) waves. Furthermore, the LIN term was shown to be more persistent than either the total heat flux anomaly or the NONLIN term, and this was attributed to the apparent extreme long persistence of the phase of wave-1 anomalies.

A key question of interest to us is whether the LIN term is primarily driven by standing waves with fixed nodes and varying amplitude or traveling waves moving in and out of phase with the climatology. This question is not a new one. For example, the introduction of Holton and Mass (1976) states "The winter seasonal mean circulation of the Northern Hemisphere consists primarily of planetary waves of zonal wavenumbers 1 and 2 superposed on a zonal westerly vortex. The planetary waves are quasi-stationary in phase but tend to fluctuate in amplitude." Continuing, the authors also reference weaker wave–mean flow oscillations that "can, to a large extent, be accounted for by the presence of traveling wave modes which alternately constructively and destructively interfere with the quasi-stationary waves." Clear examples of both behaviors can be seen in nature (see Fig. 1 of Watt-Meyer and Kushner 2015, hereafter WK15). However, to our knowledge, a quantitative decomposition of the variability of the upward wave activity flux into standing and traveling components in reanalysis data has not been made. This study makes such a decomposition by using a statistical technique that was developed by WK15 in order to decompose general wave variability into standing and traveling components. This method is an improvement on classical techniques (Hayashi 1971, 1977, 1979; Pratt 1976) because it properly accounts for the covariance between the standing and traveling waves, and because it easily allows for the reconstruction of the real-space signals. WK15 applied the decomposition to Northern Hemisphere planetary waves and showed that standing waves explain the largest portion of geopotential height variance at low frequencies and planetary wavenumbers. An exception is for wave 1 in the high-latitude troposphere, where there is a strong westward traveling wave. Furthermore, WK15 showed that the standing waves have preferred longitudes for their crests and troughs, and that at most levels and latitudes these tend to align with the extremes of the climatological wave. This suggests that these standing waves should be efficient drivers of the LIN term.

Our current study makes a quantitative decomposition of the LIN term into contributions from standing and traveling waves. We show that on time

[1] Figure 1 composites geopotential over strong (anomalously positive with respect to the climatology) and weak (anomalously negative) heat flux events. Note that during the anomalously negative events the total heat flux is still weakly positive.

scales greater than about 15 days, that is, on the time scales most important for the driving of polar vortex strength by upward wave activity flux, standing waves explain the majority of the variance of the LIN term. Furthermore, we show that because the standing waves are dominated by low frequencies (WK15) they are thus more persistent than the other components of the heat flux. We explore the implications of this for the predictability of extreme stratospheric polar vortex events. We show that polar vortex strength anomalies are preceded by persistent LIN heat fluxes in the troposphere and stratosphere that are primarily driven by standing waves. It is verified that climate models, particularly those with sufficient resolution of the stratosphere, are capable of capturing this connection between different components of the wave driving and polar vortex strength changes. Finally, we show that displacement sudden stratospheric warmings are primarily driven by standing waves forcing LIN heat flux, while split SSWs have shorter-lived heat flux precursors.

2. Data and methods

a. Data and notation

We use 1979–2013 daily-mean geopotential height, meridional wind, and temperature data from the ERA-Interim reanalysis (Dee et al. 2011). The data are on a $1.5° \times 1.5°$ latitude/longitude grid, with 37 vertical levels from 1000 to 1 hPa. Daily climatologies are computed as an average over all 35 years of the dataset for each day of the year and are denoted as A_c for some arbitrary variable A. Anomalies from the climatology are written as $A' = A - A_c$. Zonal means are written as $\{A\}$ and deviations therefrom as $A^* = A - \{A\}$. Note that unlike in WK15, we do not linearly detrend or remove the time mean of each winter season before applying the spectral analysis.

We will focus on the heat flux anomalies averaged, with a cosine of latitude weighting, between 45° and 75°N. We use this latitude range because this is where strong positive anomalies of upward wave activity flux occur before events of a weak stratospheric polar vortex (e.g., Fig. 3 of Limpasuvan et al. 2004) and because it has been used in many previous studies (e.g., Polvani and Waugh 2004). Some of our results will examine the meridional eddy heat flux at 100 hPa, as a proxy for upward wave activity flux from the troposphere to the stratosphere (Polvani and Waugh 2004), while others show the heat flux anomalies at all levels. We will use the normalized polar cap geopotential height anomaly, north of 65°N, as a proxy for the northern annular mode (NAM; Baldwin and Thompson 2009), noting that this quantity has the opposite sign as the typically defined NAM. Sudden stratospheric warmings are identified using the criteria of Charlton and Polvani (2007), including the categorization into displacement and split events. Central dates are identified by the day on which the zonal mean wind at 60°N and 10 hPa falls below zero. The categorization into split and displacement events is done according to the first column in Table 1 in Hitchcock et al. (2013), which is based on the NASA Global Modeling and Assimilation Office MERRA reanalysis. The agreement between reanalysis products in the Northern Hemisphere for the satellite era (after 1979) is such that it is acceptable to use a classification applied to a different reanalysis product [e.g., compare the two columns of Table 1 in Hitchcock et al. (2013)]. We additionally include the split event of 6 January 2013 (e.g., Tripathi et al. 2015), which occurred after the study period of Hitchcock et al. (2013). Note that the results do not differ in a qualitative sense if the event categorization from Table 1 of Cohen and Jones (2011) is used, which is based on the NCEP–NCAR reanalysis.

Part of our interest in the results described in this study is due to their implications for potential improvements in climate prediction on seasonal and longer time scales. For this reason, we verify the ability of so-called high-top and low-top climate models with different vertical resolutions in the stratosphere to capture this variability (Gerber et al. 2010). In particular, we show results based on simulations with the Canadian Middle Atmosphere Model (CMAM; Scinocca et al. 2008). These experiments were examined by Shaw et al. (2009) in order to understand the importance of momentum conservation in gravity wave drag parameterizations. Briefly, they consist of 40-yr high-top (model lid at 0.001 hPa with 71 vertical levels) and low-top (model lid at 10 hPa with 41 vertical levels) simulations.[2] CMAM is an atmosphere-only model, and in these runs interactive chemistry is turned off. Results from a model lid height comparison experiment with the Centre National de Recherches Meteorologiques climate model, CNRM-CM5 (Voldoire et al. 2013), will also be shown in the appendix.

b. Linear interference decomposition

Using the expansion of the meridional wind and temperature zonal eddies into their climatological and anomaly components, $v^* = v_c^* + v^{*\prime}$ and $T^* = T_c^* + T^{*\prime}$, the anomalous meridional heat flux can be written as (e.g., Smith and Kushner 2012)

[2] These correspond to the HIGH_C and LOW_C experiments of Shaw et al. (2009).

$$\{v^*T^*\}' = \{v^{*\prime}T^*_c\} + \{v^*_c T^{*\prime}\} + \{v^{*\prime}T^{*\prime}\}' = \text{LIN} + \text{NONLIN} \quad (1)$$

where

$$\text{LIN} = \{v^{*\prime}T^*_c\} + \{v^*_c T^{*\prime}\} \quad \text{and} \quad (2)$$

$$\text{NONLIN} = \{v^{*\prime}T^{*\prime}\} - \{v^{*\prime}T^{*\prime}\}_c = \{v^{*\prime}T^{*\prime}\}'. \quad (3)$$

Briefly, the LIN term, which has a linear dependence on the wave anomaly, represents the contribution to heat flux from wave anomalies reinforcing or attenuating the background climatological wave. It is primarily controlled by the relative phase of the anomaly and the climatology. The NONLIN term has a quadratic dependence on the wave anomaly and is largely determined by the anomaly amplitude and its vertical tilt. The variance of $\{v^*T^*\}'$ can be separated into contributions from LIN and NONLIN, and the covariance between them, using the general statistical relationship $\text{var}(A + B) = \text{var}(A) + \text{var}(B) + 2\text{cov}(A, B)$. That is,

$$\text{var}(\{v^*T^*\}') = \text{var}(\text{LIN}) + \text{var}(\text{NONLIN}) + 2\,\text{cov}(\text{LIN}, \text{NONLIN}). \quad (4)$$

c. Standing and traveling wave decomposition

To understand the structure of the wave anomalies that are driving the LIN term we will use a spectral decomposition introduced by WK15. Using a 2D discrete Fourier transform, one can represent any real longitude- and time-dependent signal $q(\lambda, t)$, defined at N equally spaced points in longitude and T days, as

$$q(\lambda, t) = \frac{2}{NT} \sum_{k=1}^{N_2} \sum_{j=-T_2}^{T_2} Q_{k,j} \cos(k\lambda + \omega_j t + \phi_{k,j}), \quad (5)$$

where k is the zonal wavenumber, j is an index that corresponds to the frequency $\omega_j = 2\pi j/T$, $N_2 = (N - 1)/2$, and $T_2 = (T - 1)/2$. For simplicity, it has been assumed that $q(\lambda, t)$ has zero zonal mean, and that N and T are odd. Note that $Q_{k,j} \geq 0$ and $-\pi < \phi_{k,j} \leq \pi$ are the amplitude and phase of the Fourier coefficient corresponding to the wavenumber and frequency pair (k, ω_j). We define the following decomposition of the Fourier amplitudes:

$$Q^{\text{St}}_{k,j} = \min(Q_{k,j}, Q_{k,-j}), \quad (6a)$$

$$Q^{\text{Tr}}_{k,j} = Q_{k,j} - Q^{\text{St}}_{k,j}. \quad (6b)$$

The superscripts St and Tr represent standing and traveling, respectively. This decomposition forces the standing portion of the wavenumber–frequency spectrum to be symmetric with respect to frequency, as desired since a pure standing wave is the sum of two oppositely propagating waves of equal phase speed and amplitude. Furthermore, Eq. (6b) ensures that the standing and traveling signals will add to the total signal. As a straightforward consequence of Eq. (6b), note that

$$(Q_{k,j})^2 = (Q^{\text{St}}_{k,j})^2 + (Q^{\text{Tr}}_{k,j})^2 + 2Q^{\text{St}}_{k,j}Q^{\text{Tr}}_{k,j}. \quad (7)$$

That is, the total power spectrum of the signal $q(\lambda, t)$ is split into three terms, representing the variance of the standing waves, the variance of the traveling waves, and the covariance between them. Previous authors (Hayashi 1971, 1977, 1979; Pratt 1976) did not explicitly account for this covariance term. Further details regarding this decomposition and the results of applying it to planetary scale waves in the Northern Hemisphere can be found in WK15.

Given the decomposition in Eq. (6) of the Fourier coefficients into standing and traveling parts, it is straightforward to use Eq. (5) to reconstruct the real-space standing and traveling parts of the signal, which we write as $q_{\text{St}}(\lambda, t)$ and $q_{\text{Tr}}(\lambda, t)$. Applying the decomposition to the meridional wind and temperature anomalies one can separate the LIN term into contributions from standing and traveling wave anomalies:

$$\text{LIN} = \text{LIN}_{\text{St}} + \text{LIN}_{\text{Tr}}, \quad (8)$$

where

$$\text{LIN}_{\text{St}} = \{v^{*\prime}_{\text{St}}T^*_c\} + \{v^*_c T^{*\prime}_{\text{St}}\} \quad \text{and} \quad (9a)$$

$$\text{LIN}_{\text{Tr}} = \{v^{*\prime}_{\text{Tr}}T^*_c\} + \{v^*_c T^{*\prime}_{\text{Tr}}\}. \quad (9b)$$

3. Results

a. Northern Hemisphere wintertime heat flux variance

Figure 2 shows the wintertime interannual variance of $\{v^*T^*\}'$ at 100 hPa and averaged between 45° and 75°N, as well the variance decomposition of the heat flux anomaly into the LIN and NONLIN terms [see Eq. (4)], and the decomposition of the LIN term into its standing and traveling parts. The top panel shows the November–March (NDJFM) mean of the daily interannual variance of the heat flux and its components. The LIN term explains about 65% of the variance of the total heat flux anomaly and the NONLIN term about 50%, and there is a negative contribution of 15% from the covariance of the LIN and NONLIN terms. This demonstrates that on daily time scales the LIN term is the most important contributor to the variability of heat flux anomalies, but

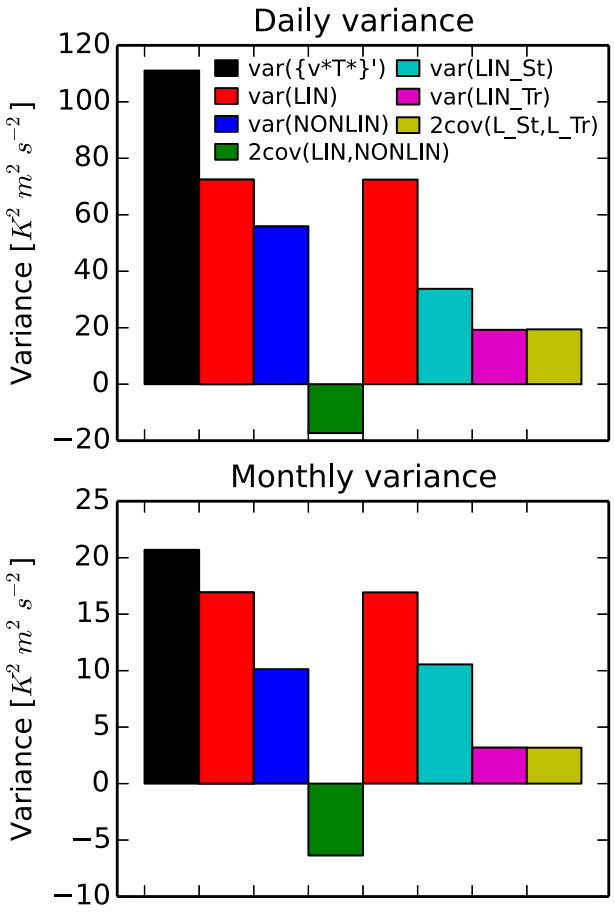

FIG. 2. The NDJFM-mean interannual variance of $\{v^*T^*\}'$ and its various components. The heat fluxes are all at 100 hPa and averaged between 45° and 75°N. (top) Interannual variance of daily heat fluxes is computed, then averaged over NDJFM. (bottom) Interannual variance of monthly heat fluxes is computed, then averaged over NDJFM.

that the NONLIN term also makes a substantial contribution. On the other hand, if, as in Smith and Kushner (2012), we first compute monthly averages of the heat fluxes before computing the interannual variance (bottom panel of Fig. 2), then the LIN term explains about 82% of the variance and the NONLIN term 49%, and there is a larger negative contribution of −31% from the covariance. Thus, for monthly heat flux anomalies, the LIN terms make a substantially larger contribution to the variance and this is compensated by a larger negative covariance. This suggests that the LIN term is more important on longer time scales. Section 3c will examine in more detail the dependence of the LIN and NONLIN terms on length of integration.

Figure 2 also shows the variance decomposition of the LIN term into its standing and traveling parts. This shows that standing wave anomalies are the primary drivers of variability of the LIN term. The bottom panel of Fig. 2 shows this is particularly true on the longer (i.e., monthly) time scales where the LIN term dominates. This is expected because the standing waves have their peak spectral power at lower frequencies than the traveling waves (see Fig. 4 of WK15). We also expect the standing waves to efficiently contribute to the LIN term because their antinodes align well with the extremes of the climatological wave at 100 hPa. This is shown for wave 1, the dominant wavenumber for the LIN term, in Fig. 3a (see also Fig. 6 of WK15). Overall, the standing wave-1 anomalies tend to be more barotropic than the climatology, with their extremes shifted to the west in the troposphere, and shifted to the east in the stratosphere. However, near 100 hPa, there is very close alignment between the standing waves and the climatology and they are able to efficiently drive the LIN term. To illustrate the impact of the standing waves more explicitly, Figs. 3b and 3c show the sum of the NDJFM-averaged wave-1 Z_c^* at 60°N and a wave-1 mode, which represents a typical standing wave in phase (Fig. 3b) and out of phase (Fig. 3c) with the climatology. This standing wave mode is constructed as follows: the phase is one of the longitudes of the extremes of the time variance, which are given as the dashed lines in Fig. 3a. For the in-phase (out of phase) standing wave the dashed line closer to the maximum (minimum) of the climatological wave is selected. The amplitude of the standing wave at each level is given by the zonal maximum of the standard deviation over all NDJFM days of $Z_{\mathrm{St}}^{*\prime}$ at that particular level. Figures 3b and 3c demonstrate that the standing waves primarily drive changes in the amplitude of the climatological wave, and additionally modify the baroclinicity of the climatological wave in the lower stratosphere and troposphere.

The greater dominance of LIN and $\mathrm{LIN_{St}}$ on monthly time scales seen in Fig. 2 suggests that they should have longer autocorrelation time scales than the total heat flux anomaly. Smith and Kushner (2012) showed that indeed the LIN term has a longer autocorrelation time scale than the total heat flux anomaly. The next section will explore the drivers of the persistence of the LIN term.

b. *Persistence of LIN heat flux anomalies*

We show the autocorrelation of various components of the heat flux anomaly at 100 hPa and 45°–75°N in Fig. 4. As was shown by Smith and Kushner (2012), the LIN heat flux is more persistent than the total heat flux anomaly, which is in turn more persistent than the NONLIN heat flux. Figure 4 additionally shows that the autocorrelation of the $\mathrm{LIN_{St}}$ term is longer than the LIN

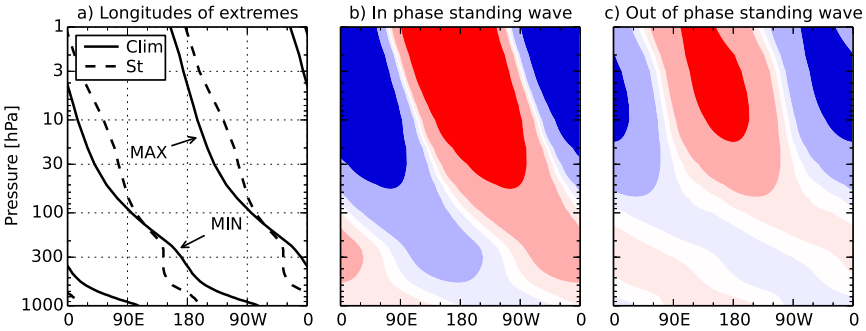

FIG. 3. (a) The longitudes of the extremes of the NDJFM-averaged wave-1 Z_c^* at 60°N (solid) and the longitudes of the zonal maxima of the time variance over all NDJFM days of wave-1 $Z_{\mathrm{St}}^{*\prime}$ at 60°N (dashed). (b) The sum of the NDJFM-averaged wave-1 Z_c^* and a wave-1 mode representing a standing wave in phase with the climatology. (c) As in (b), but for an out-of-phase standing wave. See text for details. The contours for (b) and (c) are ±20 m, ±80 m, and ±320 m.

term. The $\mathrm{LIN}_{\mathrm{Tr}}$ term has an autocorrelation similar to the $\{v^*T^*\}'$ term (i.e., is less persistent than the LIN term). These results support what was found in Fig. 2: the LIN and $\mathrm{LIN}_{\mathrm{St}}$ terms explain a larger portion of the variance of the total upward wave activity flux on monthly time scales because they are more persistent than NONLIN and $\mathrm{LIN}_{\mathrm{Tr}}$, respectively.

Smith and Kushner (2012) attributed the persistence of the LIN term to the long persistence of the phase of wave-1 $Z^{*\prime}$ (see their Fig. 6b). However, the standing and traveling wave decomposition used in this study provides a different view. It demonstrates that the slow decay of autocorrelation for the phase of wave 1 at 60°N and 100 hPa is actually primarily driven by the presence of a strong westward traveling wave in this region. This somewhat counterintuitive result will be explained below. First, the autocorrelations of the phase of the total, standing, and traveling parts of the wave-1 $Z^{*\prime}$ are shown in Fig. 5. To compute the autocorrelation of phase, we first "unwrap" each winter's time series of the phase so that there are no discontinuities greater than π.[3] We then compute the autocorrelation of this unwrapped time series. Years that have a coherent wave consistently traveling in one direction will have an unwrapped phase time series that is steadily decreasing (for a westward traveling wave) or increasing (for an eastward traveling wave). Since the autocorrelation of a time series with a pure linear trend is identically equal to 1 for any lag, this is what leads to the many winters where the autocorrelation of phase of the traveling wave 1 (Fig. 5c) has values near 1.0 for lags of up to 40 days. Similarly, it is what contributes to the apparent long persistence of the phase of the total wave 1 (Fig. 5a). However, since the persistence of the phase is due to coherent traveling waves, this means it will not necessarily enhance persistence in heat flux related to the LIN term. As an extreme case, consider a steady westward traveling wave-1 anomaly with a period of 25 days and constant amplitude. This would give a phase autocorrelation of 1.0 for any lag, but the LIN term would vary sinusoidally with the 25-day period (assuming the climatology has constant amplitude and phase). Thus, we cannot simply

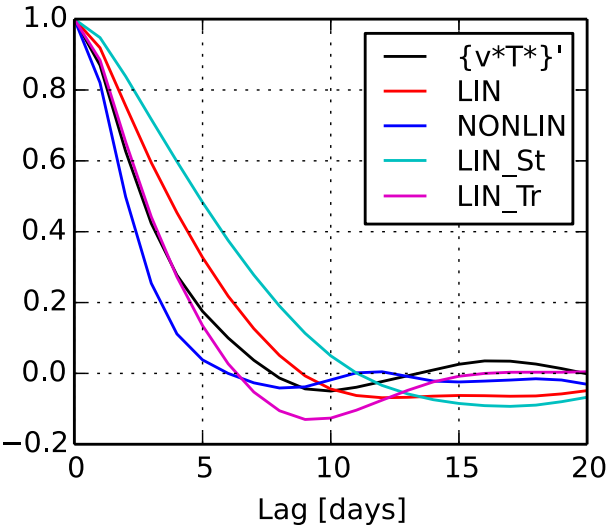

FIG. 4. The NDJFM autocorrelation of various parts of heat flux anomaly at 100 hPa and averaged between 45° and 75°N. The autocorrelation is computed separately for each winter season, and then averaged over all years.

[3] This is done as follows: proceeding through the time series by day, we first check if the difference between the next day and the current day is greater than π or less than $-\pi$. If the former, then we subtract 2π from all the days after the current day. If the latter, we add 2π to all the days after the current day. If neither, we do nothing and proceed to the next day.

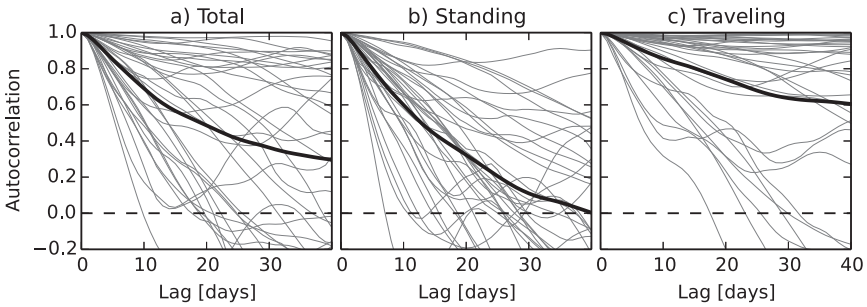

FIG. 5. NDJFM autocorrelation of the phase of wave-1 $Z^{*\prime}$ at 60°N and 100 hPa: (a) the total $Z^{*\prime}$, (b) the standing part of $Z^{*\prime}$, and (c) the traveling part of $Z^{*\prime}$. Thin gray lines are the individual autocorrelations computed over each winter season, and the thick black line is the average of the autocorrelations over all winter seasons.

attribute the longer persistence of the LIN term in Fig. 4 to the long phase persistence seen in Fig. 5a.

Nevertheless, despite the discussion above, Fig. 5b shows that the standing wave anomaly still has a relatively long phase persistence, with an autocorrelation value of about 0.3 after a lag of 20 days. This is substantially longer than the autocorrelation of the amplitude of wave-1 anomalies (cf. Fig. 6b of Smith and Kushner 2012). The standing wave phase autocorrelation is representative of how long standing anomalies tend to be fixed in place, and it shows that the low-frequency standing waves are driving the persistence of the LIN heat flux.

c. *Sensitivity of vertical wave activity flux to pulse duration*

Figure 6 shows the average heat flux anomaly and the LIN and NONLIN terms during periods of extreme heat flux anomaly, as a function of integration length. For a given integration length N, we find the periods of most extreme $\{v^*T^*\}'$ averaged over N days for each NDJFM season. We then compute the average over all winter

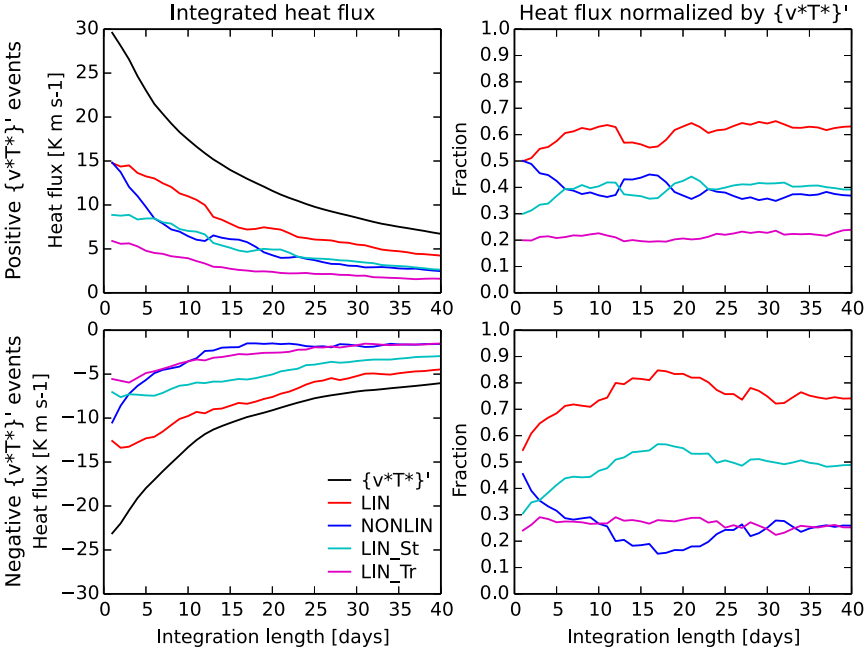

FIG. 6. The average heat flux anomaly over the most extreme N-day running mean of each winter. For each winter season we compute an N-day running mean of $\{v^*T^*\}'$ and then find the days of the most extreme (top) positive and (bottom) negative anomalies. The values of $\{v^*T^*\}'$, LIN, NONLIN, $\mathrm{LIN_{St}}$, and $\mathrm{LIN_{Tr}}$ are then composited over each winter's extreme event. Results are shown for (left) the actual mean heat flux during the period and (right) the heat flux normalized by the total heat flux anomaly.

seasons of $\{v^*T^*\}'$, LIN, NONLIN, LIN_{St}, and LIN_{Tr} during these periods. This shows the contribution of different terms during periods of extreme heat flux anomaly of differing lengths. The left column in Fig. 6 shows the actual heat fluxes during the events, while the right column shows various components of the heat flux normalized by the total heat flux anomaly. For the daily ($N = 1$) composites, the average positive heat flux anomaly is about $30\,\text{K m s}^{-1}$ while the average negative heat flux anomaly is about $-23\,\text{K m s}^{-1}$. This difference is due to the positive skewness of the heat flux distribution (not shown). As the averaging period becomes longer, the mean heat flux during the average period decreases in an absolute sense for both the positive and negative heat flux events. The daily (i.e., $N = 1$) heat flux events have equal contributions from the LIN and NONLIN terms for the positive events, while there is a greater contribution from the LIN term for the negative events. As the integration length increases to 20 days, a larger portion of the heat flux comes from the LIN term. This occurs for both the positive and negative heat flux events, but the change is greater for the negative events: for an integration length of 17 days, 85% of the heat flux anomaly is contributed by the LIN term. The positive heat flux events generally have at most 65% of their value contributed by the LIN term. Between 20 and 40 days, the relative portions explained by the LIN and NONLIN terms stay roughly constant, with a slight decrease in the LIN term for the negative events. The changes in the LIN heat flux as the integration length changes are primarily driven by the standing portion of the LIN term. The traveling wave part remains constant at around 20%–25% over all integration lengths.

These changes in the relative importance of the components of the heat flux as a function of pulse duration confirm what was seen in Fig. 2. There we saw that the LIN and LIN_{St} terms explain a larger portion of the variance of the total heat flux on monthly time scales than on daily time scales. Figure 6 confirms that for extreme events the same holds true: on longer (>15 day) time scales, the LIN and LIN_{St} terms are a larger portion of heat flux pulses, at the expense of the NONLIN term. The decomposition of extreme heat flux pulses into LIN and NONLIN terms for $N = 40$ was previously examined in Smith and Kushner (2012), who showed that, in agreement with our results, negative heat flux anomalies are more driven by the LIN term than positive heat flux anomalies (see their Fig. 3).

d. *Polar vortex strength connection to upward wave activity flux*

We now show the connection between different components of the heat flux anomaly and polar vortex strength, as diagnosed by the NAM at 10 hPa. Given that LIN_{St} is the most persistent part of the heat flux anomaly, we expect it to be most well correlated with changes in the stratospheric NAM. This follows from the fact that polar vortex strength changes are driven by relatively long-lasting pulses of upward wave activity (Polvani and Waugh 2004; Sjoberg and Birner 2014). Figure 7 shows the lag correlations of various quantities with the NAM at 10 hPa, as a function of pressure. Focusing first on the correlation of the NAM with itself (Fig. 7a) we see the well-known slow downward propagation of NAM anomalies through the stratosphere, with persistent connections to the surface. Figure 7b shows that a weakened (strengthened) stratospheric polar vortex is typically preceded by anomalously high (low) upward wave activity flux in the stratosphere for a period of about 40 days. There is a weaker opposite signed response in the upward wave activity flux for positive lags. The total heat flux correlations for negative lags are primarily confined to the stratosphere (above 200 hPa).

Comparing Figs. 7c and 7d shows that the correlations of the LIN and NONLIN terms with the stratospheric NAM have very different structures. In general the LIN correlations are similar to the total heat flux anomaly correlations, suggesting that the connection between upward wave activity flux and polar vortex strength is primarily driven by waves amplifying or attenuating the background climatology. Furthermore, the LIN term also has significant positive correlations in the troposphere for lags of up to −30 days, while the NONLIN term only has positive correlations above about 200 hPa. This shows that the LIN term is responsible for driving the connection between upward wave activity flux generated in the troposphere and polar vortex strength. Finally, the correlations of the LIN term are dominated by the standing wave contribution. This is seen in Figs. 7e and 7f: the LIN_{St} correlation pattern is very similar to the total LIN pattern, while the LIN_{Tr} correlations are more short-lived and weaker.

Figure 7b showed that correlations between tropospheric heat flux and stratospheric polar vortex strength are very weak to nonexistent. However, we know from Charney and Drazin (1961) that only waves with the largest horizontal scales are able to propagate from the troposphere to stratosphere during typical winter conditions. For this reason, we additionally show the correlations for the wave-1 component of $\{v^*T^*\}'$ and LIN in Figs. 7g and 7h. A stronger (>0.2) correlation is now seen between tropospheric heat flux and the 10-hPa NAM, especially for lags of −15 to −40 days. There is also a weak positive correlation in the troposphere at a lag of more than a month, before the peak stratospheric

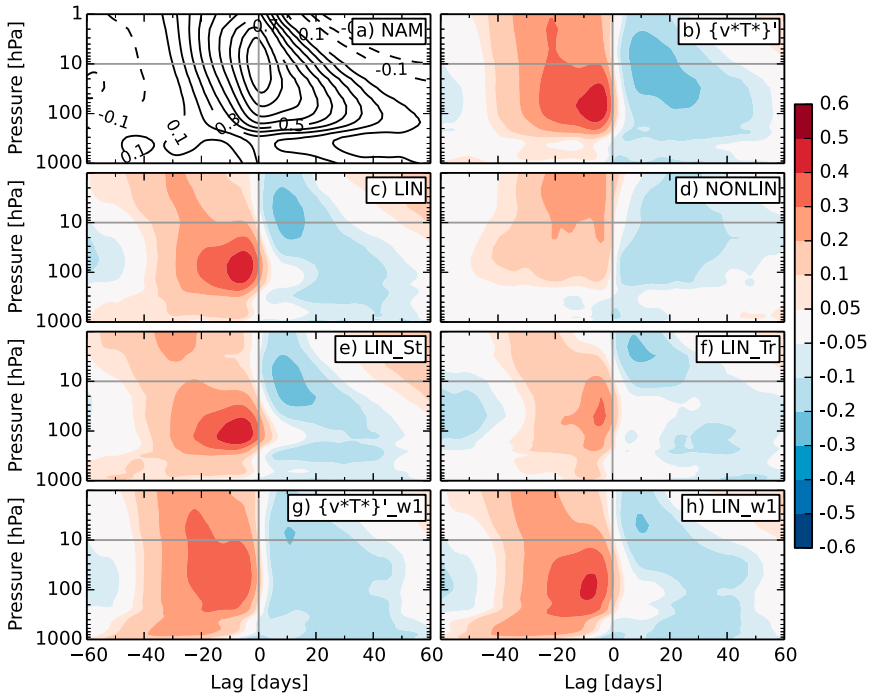

FIG. 7. Lag correlation as a function of height of various quantities with the NAM at 10 hPa in the ERA-Interim reanalysis. Computed from all NDJFM 1979–2013 days. (a) Lag correlation of NAM at various heights with the NAM at 10 hPa, contour intervals are 0.1, with the zero contour omitted. All other panels are the lag-correlation of different components of heat flux anomaly at various heights with the NAM at 10 hPa: (b) total heat flux anomaly, (c) LIN, (d) NONLIN, (e) LIN_{St}, (f) LIN_{Tr}, (g) wave-1 heat flux anomaly, and (h) wave-1 LIN.

signal. The correlations of the wave-1 component of LIN are very similar to the total wave-1 heat flux anomaly. The NONLIN correlations are weak throughout for wave 1 and the wave-1 LIN correlations are primarily due to the standing wave part (not shown).

We estimate the statistical significance of the preceding lag correlations using a method described in Lau and Chan (1983). This technique calculates a confidence interval by assuming each time series is a first-order Markov processes and computing their autocorrelation time scales. Thus, the statistical significance of the correlations will vary depending on the predictor variable, and also be a function of height and lag (since for greater lags there are fewer data points with which to compute the correlations). See Lau and Chan (1983) for details of the computation. Broadly speaking, the lag correlations of the NAM with itself (Fig. 7a) are significant at the 95% level at values of 0.10 to 0.13 in the troposphere and upper stratosphere, and at 0.12 to 0.16 in the lower stratosphere where the NAM is most persistent. The lag correlations between the heat fluxes and the NAM (Figs. 7b–h) are significant at 95% for lower values of the correlation because the heat flux is less persistent than the NAM. The total heat flux anomaly correlations (Fig. 7b) are significant for values of about 0.05 to 0.07 in the troposphere, and 0.07 to 0.10 in the stratosphere. The other correlations are significant at approximately the same values for the NONLIN term, and at slightly higher values for LIN and wave-1 components since they are more persistent.

e. *Vortex strength connection to wave activity flux in models*

Figures 8 and 9 show the same diagnostics as Fig. 7 for, respectively, the high-top and low-top versions of the CMAM model. It is apparent that the simulations with the high-top version of the model (Fig. 8) broadly capture the same lag-correlation structure seen in the ERA-Interim reanalysis. The primary difference is that the heat flux correlations are slightly higher in the CMAM simulations for lags of −20 to 0 days. This is especially for the LIN_{Tr}, which causes the correlations for LIN_{St} and LIN_{Tr} to be more similar for CMAM as compared to ERA-Interim. This is in accordance with the fact that LIN_{Tr} explains a slightly larger portion of the variance of LIN in the high-top CMAM compared to ERA-Interim, and that the LIN_{St} and LIN_{Tr} terms have more similar persistence time scales in the model simulations (not

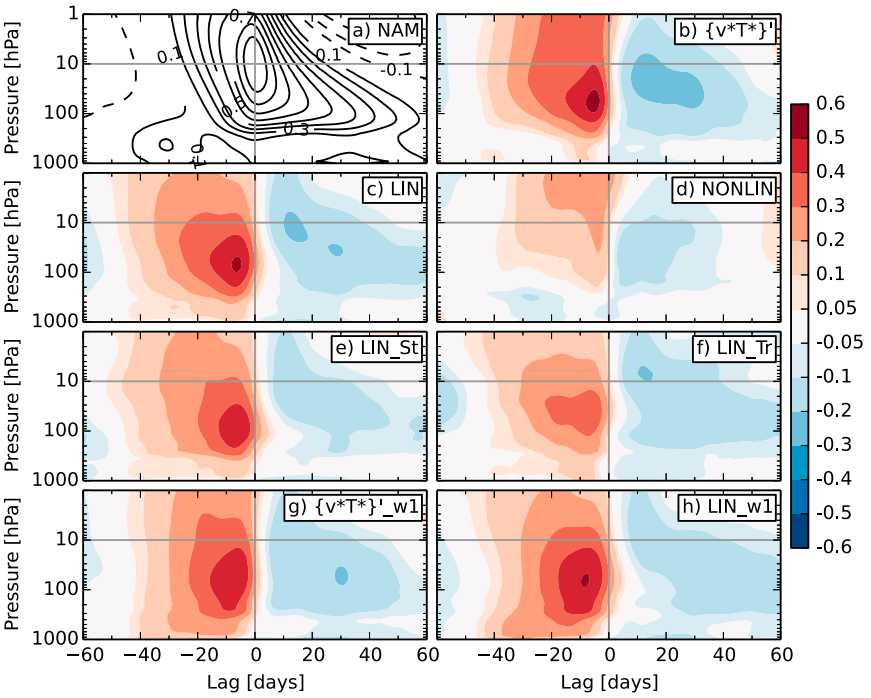

FIG. 8. As in Fig. 7, but for the high-top version of the CMAM model. Computed from 40 years of NDJFM days.

shown). On the other hand, the lag correlations in the low-top version of the CMAM model (Fig. 9) are markedly different from those seen in the reanalysis. In general the heat flux correlations for negative lags are too large and begin at earlier lags than in ERA-Interim. This is particularly true for the LIN and LIN_{St} terms, and less so for the LIN_{Tr} term. Furthermore, there is no significant correlation between NONLIN and the

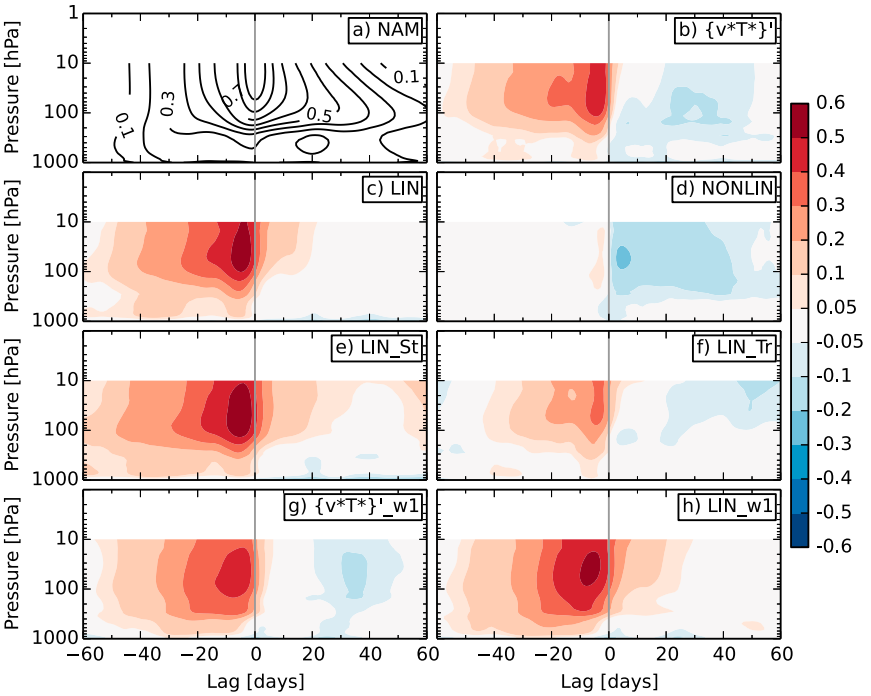

FIG. 9. As in Fig. 8, but for the low-top version.

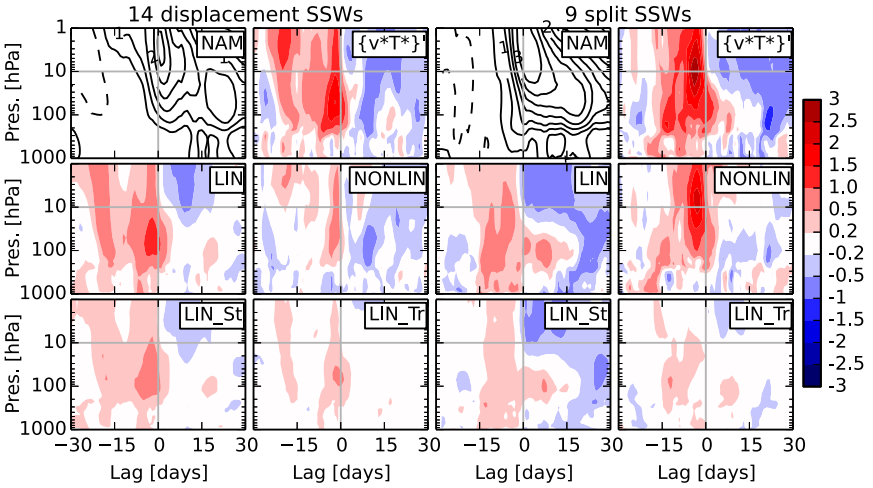

FIG. 10. Composite of NAM and heat fluxes over (left) 14 displacement SSWs and (right) 9 split SSWs in the 1979–2013 ERA-Interim reanalysis. All of the heat fluxes are normalized by the level-dependent standard deviation of $\{v^*T^*\}'$, computed over all NDJFM days. The contour intervals for the NAM panels are 0.5, with the zero contour omitted.

stratospheric NAM for negative lags. And finally, there is a lack of negative correlations between the heat flux and NAM for positive lags, except for the NONLIN term. This comparison of high-top and low-top simulations demonstrates the importance of simulating the stratosphere for properly representing the influence of upward wave activity flux on the polar vortex strength. It also shows that the connections found in the ERA-Interim reanalysis can be reasonably well represented by a model with a well-resolved stratosphere.

f. Linear interference and SSWs

The extremes of stratospheric variability are particularly important to be able to predict because they tend to be followed by persistent anomalies in the troposphere (e.g., Sigmond et al. 2013). In this section we show the heat flux precursors to sudden stratospheric warmings (SSWs) in the reanalysis for 1979–2013. This was shown for the LIN and NONLIN terms in Smith and Kushner (2012), and here we extend the analysis to the $\mathrm{LIN}_{\mathrm{St}}$ and $\mathrm{LIN}_{\mathrm{Tr}}$ components.[4] We make separate composites over displacement and split SSWs as discussed in section 2a. Figure 10 shows the composite of the NAM and various components of the heat flux at all levels, from 30 days preceding to 30 days following displacement and split SSWs. The NAM panels show the strong deceleration of the polar vortex, with NAM values exceeding 3 and 3.5 standard deviations for the displacement and split composites, respectively. As expected, preceding the SSW events are anomalously large values of upward wave activity flux for lags of up to 25 days, throughout the stratosphere and intermittently in the troposphere. The displacement events show a persistent anomaly exceeding one standard deviation for about 25 days before the event, and a stronger positive anomaly of up to two standard deviations in the lower stratosphere for lags of −5 to 0 days. The split events on the other hand have weaker precursors from lags of −25 to −10 days, but are preceded by heat flux anomalies of above two standard deviations throughout lower to middle stratosphere from −8 to −2 days lag.

The second row of Fig. 10 shows the LIN and NONLIN signatures associated with the displacement and split SSWs. The persistent heat flux anomaly preceding displacement events is largely made up of the LIN term, with a short contribution from the NONLIN term just before lag 0. The split events have a weaker LIN signature for negative lags, in agreement with the weaker total heat flux precursors at longer lags associated with the split events, but have a much larger contribution from the NONLIN term for about 7 days preceding the events. The third row of Fig. 10 shows the composites of $\mathrm{LIN}_{\mathrm{St}}$ and $\mathrm{LIN}_{\mathrm{Tr}}$ during the SSW events. This demonstrates that the positive LIN anomaly preceding displacement SSWs is primarily driven by standing waves. Overall, Fig. 10 shows that displacement events have longer lead-time heat flux precursors, which consist of an amplification of the climatological wave by a standing wave anomaly. On the other hand, split events have a stronger but short-lived heat flux signature, which is a

[4] Smith and Kushner (2012) showed composites over SSW events in the 1958–2009 period in the NCEP–NCAR reanalysis.

result of the wave anomaly interacting with itself (i.e., the NONLIN term). This suggests that displacement events may be more predictable than split events, and that tracking the standing wave field would be important for the prediction of displacement SSWs.

4. Conclusions and discussion

This study examined whether standing or traveling waves primarily drive the linear interference effect. It was shown that standings waves explain the largest portion of the variance of the LIN term. This is because the standing waves are well aligned with the climatology, and hence can efficiently drive amplifications and attenuations of the climatological wave. The standing waves are also dominated by low frequencies, and have a long-lived phase persistence. Because of this, the standing part of the LIN term has a longer autocorrelation time scale than the other components of the upward wave activity flux. Consequently, it also explains a larger portion of the variance on monthly time scales than on daily time scales. This also holds for extreme heat flux anomalies: as the duration of wave activity pulses increases, a larger portion is explained by the LIN and LIN_{St} terms.

The fact that standing waves drive the most persistent part of the wave activity flux suggests that they should be primarily responsible for the connection between wave driving and stratospheric polar vortex strength. This is confirmed in reanalysis data, and it is verified that an atmospheric model with a well-resolved stratosphere is able to simulate this connection well. Furthermore, the correlations between the LIN term and the polar vortex strength in the reanalysis data show clear tropospheric precursors preceding polar vortex strength by about a month. This connection is dominated by the wave-1 component of the LIN term. Finally, the upward wave activity flux precursors of SSWs are computed. As expected, weakening of the polar vortex is preceded by anomalously large upward wave activity flux. However, the duration and form of this flux depends on the type of SSW. Displacement events have longer-lived precursors which are primarily driven by the LIN term being forced by standing waves. On the other hand, split SSWs have shorter wave activity flux precursors, and they are dominated by the NONLIN term.

Some previous studies have considered the impact of traveling waves interfering with a stationary or ''quasi-stationary'' background wave (Madden 1975; Holton and Mass 1976; Lindzen et al. 1982; Salby and Garcia 1987). They have used theory, mechanistic models, and observational data to understand this effect, but are actually studying a somewhat different phenomenon than the focus of this work. Here, we decompose the wave anomaly into standing and traveling components, and quantify how each of these terms interferes with the climatology and drives the LIN term. The studies cited above take a different approach: they consider just the separation of waves into a stationary (either a climatological or a time-mean component) part and an anomaly that is assumed to be traveling with some fixed phase speed. However, as we have shown, typical wave anomalies in the atmosphere consist of standing-type variability and traveling-type variability. Hence, we believe our analysis is more complete, and is applicable to understanding the linear interference phenomenon as discussed in the introduction. Nevertheless, it would be interesting to apply the standing and traveling wave decomposition to the total wave fields (climatology + anomaly) and directly investigate the role of each of these wave types without invoking interference between the climatology and anomalies.

A practical implication of the results shown in this study is the potential for longer-range prediction of polar vortex strength changes, and consequently the subseasonal prediction of the wintertime tropospheric NAM. Clear tropospheric precursors in upward wave activity flux have been found to lead NAM changes in the stratosphere by a month. These precursors are dominated by standing waves driving the LIN term. This suggests that dynamical prediction systems must accurately represent the climatological wave structure and the standing wave anomalies to properly model this coupling. In addition, monitoring of the LIN term and the standing wave structure may be helpful for predicting polar vortex strength changes. To make such a scheme practical operationally, additional technical work is needed to extract standing and traveling signals using a digital filter in the time domain rather than in the frequency domain.

Acknowledgments. The authors acknowledge the support of the Natural Sciences and Engineering Research Council of Canada.

APPENDIX

CNRM-CM5 Model Results

Here we show the lag correlations of various heat flux components and the stratospheric NAM as in section 3e, but for simulations with the CNRM-CM5 model (Voldoire et al. 2013).[5] These unpublished runs were

[5] Note that the experiments analyzed were not run with the same resolution as the simulations discussed in Voldoire et al. (2013).

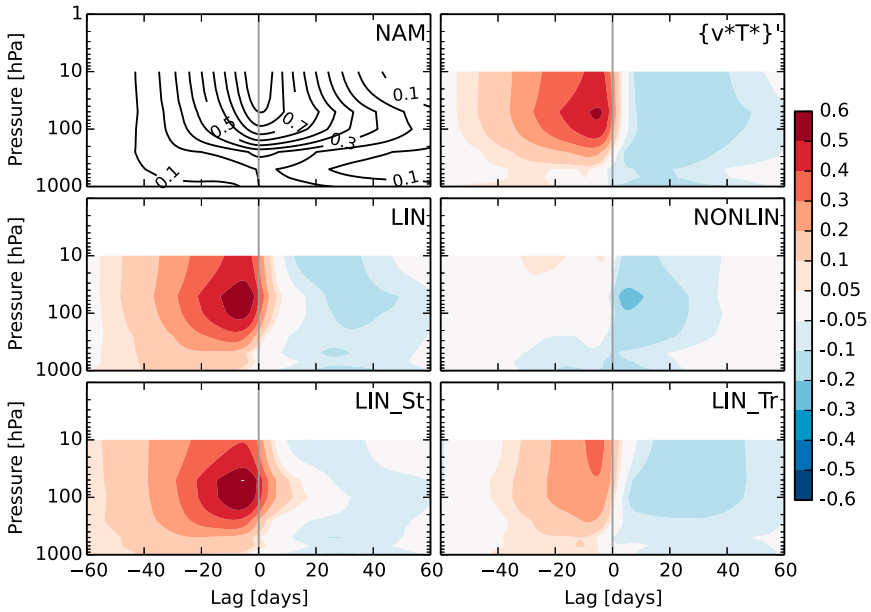

FIG. A1. Lag correlation as a function of height of various quantities with the NAM at 10 hPa in the CNRM-CM5 high-top model. Computed from 450 NDJFM seasons spanning 1981–2010. Lag correlation of NAM at various heights with the NAM at 10 hPa, contour intervals are 0.1, with the zero contour omitted, is shown at top left; all other panels are the lag correlation of different components of heat flux anomaly at various heights with the NAM at 10 hPa.

performed in order to investigate the dependence of decadal predictability on stratospheric resolution. The high-top version has 91 vertical levels up to 0.01 hPa, and the low-top version has 62 vertical levels to 5 hPa. Both have a horizontal resolution of T63. Ten realizations were run for 10 years each, starting 1 January 1981, 1986, 1991, 1996, and 2001. Thus, 450 complete NDJFM winter seasons that span the years 1981–2010 are available for each version of the model. Figure A1 shows the lag correlations between various components of the heat flux anomaly and the NAM at 10 hPa for the high-top version of the model. Compared to the ERA-Interim reanalysis, the correlations between the total heat flux anomaly and the NAM are similar, but in general slightly too strong and also begin at too large of a negative lag. This also holds for the LIN and LIN_{St} correlations. As well, there is no significant correlation between the NONLIN term and the NAM for negative correlations in the stratosphere, which is markedly different than the results for the reanalysis, and the high-top version of CMAM. This suggests that despite the good stratospheric resolution in the high-top version of CNRM-CM5, it is still not properly representing some aspect of the large-scale dynamics. Finally, the LIN correlations are strongly dominated by the LIN_{St} component, whereas the LIN_{Tr} correlations are much weaker and shorter-lived. The low-top version of the CNRM-CM5 model has very similar results, with just slightly stronger correlations seen for negative lags for the total heat flux anomaly and the LIN terms (not shown).

REFERENCES

Baldwin, M. P., and T. J. Dunkerton, 2001: Stratospheric harbingers of anomalous weather regimes. *Science*, **294**, 581–584, doi:10.1126/science.1063315.

——, and D. W. J. Thompson, 2009: A critical comparison of stratosphere–troposphere coupling indices. *Quart. J. Roy. Meteor. Soc.*, **135**, 1661–1672, doi:10.1002/qj.479.

Charlton, A. J., and L. M. Polvani, 2007: A new look at stratospheric sudden warmings. Part I: Climatology and modeling benchmarks. *J. Climate*, **20**, 449–469, doi:10.1175/JCLI3996.1.

Charney, J. G., and P. G. Drazin, 1961: Propagation of planetary-scale disturbances from the lower into the upper atmosphere. *J. Geophys. Res.*, **66**, 83–109, doi:10.1029/JZ066i001p00083.

Cohen, J., and J. Jones, 2011: Tropospheric precursors and stratospheric warmings. *J. Climate*, **24**, 6562–6572, doi:10.1175/2011JCLI4160.1.

Dee, D. P., and Coauthors, 2011: The ERA-Interim reanalysis: Configuration and performance of the data assimilation system. *Quart. J. Roy. Meteor. Soc.*, **137**, 553–597, doi:10.1002/qj.828.

Garfinkel, C., D. Hartmann, and F. Sassi, 2010: Tropospheric precursors of anomalous Northern Hemisphere stratospheric polar vortices. *J. Climate*, **23**, 3282–3299, doi:10.1175/2010JCLI3010.1.

Gerber, E. P., and Coauthors, 2010: Stratosphere–troposphere coupling and annular mode variability in chemistry–climate

models. *J. Geophys. Res.*, **115**, D00M06, doi:10.1029/2009JD013770.

Harnik, N., 2009: Observed stratospheric downward reflection and its relation to upward pulses of wave activity. *J. Geophys. Res.*, **114**, D08120, doi:10.1029/2008JD010493.

Hayashi, Y., 1971: A generalized method of resolving disturbances into progressive and retrogressive waves by space Fourier and time cross-spectral analyses. *J. Meteor. Soc. Japan*, **49**, 125–128.

——, 1977: On the coherence between progressive and retrogressive waves and a partition of space–time power spectra into standing and traveling parts. *J. Appl. Meteor.*, **16**, 368–373, doi:10.1175/1520-0450(1977)016<0368:OTCBPA>2.0.CO;2.

——, 1979: A generalized method of resolving transient disturbances into standing and traveling waves by space–time spectral analysis. *J. Atmos. Sci.*, **36**, 1017–1029.

Hitchcock, P., T. G. Shepherd, and G. L. Manney, 2013: Statistical characterization of Arctic polar-night jet oscillation events. *J. Climate*, **26**, 2096–2116, doi:10.1175/JCLI-D-12-00202.1.

Holton, J. R., and C. Mass, 1976: Stratospheric vacillation cycles. *J. Atmos. Sci.*, **33**, 2218–2225, doi:10.1175/1520-0469(1976)033<2218:SVC>2.0.CO;2.

Lau, K.-M., and P. H. Chan, 1983: Short-term climate variability and atmospheric teleconnections from satellite-observed outgoing longwave radiation. Part II: Lagged correlations. *J. Atmos. Sci.*, **40**, 2751–2767, doi:10.1175/1520-0469(1983)040<2751:STCVAA>2.0.CO;2.

Limpasuvan, V., D. W. J. Thompson, and D. L. Hartmann, 2004: The life cycle of the Northern Hemisphere sudden stratospheric warmings. *J. Climate*, **17**, 2584–2596, doi:10.1175/1520-0442(2004)017<2584:TLCOTN>2.0.CO;2.

Lindzen, R. S., B. Farrell, and D. Jacqmin, 1982: Vacillations due to wave interference: Applications to the atmosphere and to annulus experiments. *J. Atmos. Sci.*, **39**, 14–23, doi:10.1175/1520-0469(1982)039<0014:VDTWIA>2.0.CO;2.

Madden, R. A., 1975: Oscillations in the winter stratosphere: Part 2. The role of horizontal eddy heat transport and the interaction of transient and stationary planetary scale waves. *Mon. Wea. Rev.*, **103**, 717–729, doi:10.1175/1520-0493(1975)103<0717:OITWSP>2.0.CO;2.

Newman, P. A., E. R. Nash, and J. E. Rosenfield, 2001: What controls the temperature of the Arctic stratosphere during the spring. *J. Geophys. Res.*, **106**, 19 999–20 010, doi:10.1029/2000JD000061.

Nishii, K., H. Nakamura, and T. Miyasaka, 2009: Modulations in the planetary wave field induced by upward-propagating Rossby wave packets prior to stratospheric wudden warming events: A case study. *Quart. J. Roy. Meteor. Soc.*, **135**, 39–52, doi:10.1002/qj.359.

Polvani, L. M., and D. W. Waugh, 2004: Upward wave activity flux as a precursor to extreme stratospheric events and subsequent anomalous surface weather regimes. *J. Climate*, **17**, 3548–3554, doi:10.1175/1520-0442(2004)017<3548:UWAFAA>2.0.CO;2.

Pratt, R. W., 1976: The interpretation of space–time spectral quantities. *J. Atmos. Sci.*, **33**, 1060–1066, doi:10.1175/1520-0469(1976)033<1060:TIOSTS>2.0.CO;2.

Salby, M. L., and R. R. Garcia, 1987: Vacillations induced by interference of stationary and traveling planetary waves. *J. Atmos. Sci.*, **44**, 2679–2711, doi:10.1175/1520-0469(1987)044<2679:VIBIOS>2.0.CO;2.

Scinocca, J. F., N. A. McFarlane, M. Lazare, J. Li, and D. Plummer, 2008: The CCCma third generation AGCM and its extension into the middle atmosphere. *Atmos. Chem. Phys.*, **8**, 7055–7074, doi:10.5194/acp-8-7055-2008.

Shaw, T. A., M. Sigmond, T. G. Shepherd, and J. F. Scinocca, 2009: Sensitivity of simulated climate to conservation of momentum in gravity wave drag parameterization. *J. Climate*, **22**, 2726–2742, doi:10.1175/2009JCLI2688.1.

Sigmond, M., J. F. Scinocca, V. V. Kharin, and T. G. Shepherd, 2013: Enhanced seasonal forecast skill following stratospheric sudden warmings. *Nat. Geosci.*, **6**, 98–102, doi:10.1038/ngeo1698.

Sjoberg, J. P., and T. Birner, 2012: Transient tropospheric forcing of sudden stratospheric warmings. *J. Atmos. Sci.*, **69**, 3420–3432, doi:10.1175/JAS-D-11-0195.1.

——, and ——, 2014: Stratospheric wave–mean flow feedbacks and sudden stratospheric warmings in a simple model forced by upward wave activity flux. *J. Atmos. Sci.*, **71**, 4055–4071, doi:10.1175/JAS-D-14-0113.1.

Smith, K. L., and P. J. Kushner, 2012: Linear interference and the initiation of extratropical stratosphere–troposphere interactions. *J. Geophys. Res.*, **117**, D13107, doi:10.1029/2012JD017587.

Thompson, D. W. J., M. P. Baldwin, and J. M. Wallace, 2002: Stratospheric connection to Northern Hemisphere wintertime weather: Implications for prediction. *J. Climate*, **15**, 1421–1428, doi:10.1175/1520-0442(2002)015<1421:SCTNHW>2.0.CO;2.

Tripathi, O. P., and Coauthors, 2015: The predictability of the extratropical stratosphere on monthly time-scales and its impact on the skill of tropospheric forecasts. *Quart. J. Roy. Meteor. Soc.*, **141**, 987–1003, doi:10.1002/qj.2432.

Voldoire, A., and Coauthors, 2013: The CNRM-CM5.1 global climate model: Description and basic evaluation. *Climate Dyn.*, **40**, 2091–2121, doi:10.1007/s00382-011-1259-y.

Watt-Meyer, O., and P. J. Kushner, 2015: Decomposition of atmospheric disturbances into standing and traveling components, with application to Northern Hemisphere planetary waves and stratosphere–troposphere coupling. *J. Atmos. Sci.*, **72**, 787–802, doi:10.1175/JAS-D-14-0214.1.